

2018

CFD Simulation Of Vortex Flashing Flows In Convergent-Divergent Nozzles

Jingwei Zhu

ACRC, University of Illinois at Urbana-Champaign, jzhu50@illinois.edu

Stefan Elbel

elbel@illinois.edu

Follow this and additional works at: <https://docs.lib.purdue.edu/iracc>

Zhu, Jingwei and Elbel, Stefan, "CFD Simulation Of Vortex Flashing Flows In Convergent-Divergent Nozzles" (2018). *International Refrigeration and Air Conditioning Conference*. Paper 1854.

<https://docs.lib.purdue.edu/iracc/1854>

This document has been made available through Purdue e-Pubs, a service of the Purdue University Libraries. Please contact epubs@purdue.edu for additional information.

Complete proceedings may be acquired in print and on CD-ROM directly from the Ray W. Herrick Laboratories at <https://engineering.purdue.edu/Herrick/Events/orderlit.html>

CFD Simulation Of Vortex Flashing Flows In Convergent-Divergent Nozzles

Jingwei ZHU, Stefan ELBEL*

Department of Mechanical Science and Engineering,
University of Illinois at Urbana-Champaign,
1206 West Green Street, Urbana, IL, 61801, USA
Phone: (217) 244-1531, Fax: (217) 333-1942, Email: elbel@illinois.edu

* Corresponding Author

ABSTRACT

Vortex control is a novel two-phase convergent-divergent nozzle restrictiveness control mechanism by adjustable nozzle inlet vortex. It requires no change to the physical dimensions of the nozzle geometry. The control range of inlet pressures and mass flow rates that can be achieved by vortex control appears to be large enough to be suitable for numerous technical applications. This novel mechanism can potentially provide flow control with less sacrifice of nozzle efficiency, which is important in applications such as ejector cycles. It is also less vulnerable to clogging since the flow control is achieved without changing the flow area. However, the underlying mechanism behind the vortex control is still unclear. In this study, 3D CFD simulation of vortex flashing flows in convergent-divergent nozzles has been conducted in order to understand the vortex control effect. The simulation results show increase of nozzle restrictiveness after the application of inlet vortex and the predicted mass flow rates agree well with the experimental results under the same inlet and outlet conditions. More vapor has been generated in the divergent part of the nozzle after the inlet vortex is applied. Due to the much lower density of vapor compared to the liquid, when vortex is applied vapor bubbles are driven towards the nozzle center. Sensible heat of the liquid closer to the nozzle center can now be more utilized for bubble growth. It is believed that due to the more available liquid sensible heat, after the introduction of inlet vortex, vapor generation in the nozzle divergent part has thus been increased and flow control can be achieved.

1. INTRODUCTION

Refrigerant flow control with expansion devices is beneficial to the performance and reliability of air conditioning and refrigeration systems under changing working conditions. The most widely used expansion devices that regulate the refrigerant flow into the evaporators are thermostatic expansion valves (TXV) and electronic expansion valves (EEV). In systems with subcritical heat rejection, they control the superheating level at the evaporator outlet which leads to the best use of evaporator under each condition and prevents unevaporated refrigerant liquid from reaching the compressor. The flow control is accomplished by varying the expansion valve opening.

Zhu and Elbel (2016, 2017, 2018a) proposed to apply vortex at the nozzle inlet to control the nozzle restrictiveness on initially subcooled flashing flow expanded through convergent-divergent nozzles. This novel two-phase nozzle restrictiveness control mechanism by adjustable nozzle inlet vortex, called vortex control, requires no change to the physical dimensions of the nozzle geometry. A nozzle with inlet vortex was called vortex nozzle (or swirl nozzle). Zhu and Elbel's experiments on vortex nozzle with initially subcooled R134a showed that the strength of the nozzle inlet vortex can change the restrictiveness of the two-phase convergent-divergent nozzle without the need of changing the nozzle geometry. The nozzle becomes more restrictive as the strength of the vortex increases. With vortex control, the mass flow rate can be reduced by 42% under the same inlet and outlet conditions (Zhu and Elbel, 2018a). The control range of inlet pressures and mass flow rates that can be achieved by vortex control appears to be large enough to be suitable for numerous technical applications. This novel mechanism can potentially provide flow control with less sacrifice of nozzle efficiency, which is extremely important for ejector cooling cycle performance. It is also less vulnerable to clogging since the flow control is achieved without changing the flow area. A variety of

different expansion devices, in addition to ejectors, could potentially benefit from this new control mechanism, including actively controlled flow metering devices for superheat control in subcritical applications or high-side pressure control in transcritical systems. Furthermore, the new vortex control mechanism can possibly lead to alternative self-regulating expansion valve designs.

Through the literature review, it was found that flashing flow of initially subcooled or saturated fluid was studied without vortex applied, and vortex flow was mostly studied without phase change or the focus of research was on the spray dynamics and atomization characteristics. Little knowledge is available regarding the underlying mechanism behind the control effect of vortex on the flashing flow rate. In this study, 3D CFD simulation of vortex flashing flows in convergent-divergent nozzles using ANSYS CFX has been conducted. The simulation results show increase of nozzle restrictiveness after the application of inlet vortex and the predicted mass flow rates agrees well with the experimental results under the same inlet and outlet conditions. The vortex control mechanism has also been explained with the insight provided by the CFD simulation.

2. MODELS

2.1 Two-Fluid Model

The governing set of equations is the Eulerian two-fluid model at steady state with phase change, which comprises of mass, momentum and energy balances for each phase. The model assumes continuous liquid phase containing spherical particles of dispersed vapor phase.

The continuity equation for each phase is

$$\nabla \cdot (\alpha_k \rho_k \mathbf{v}_k) = \Gamma_k \quad (1)$$

with the interfacial mass transfer condition

$$\sum_{k=1}^2 \Gamma_k = 0 \quad (2)$$

Γ_k represents the rate of production of kth-phase mass from the phase changes at the interfaces per unit volume. The momentum equation for each phase is

$$\nabla \cdot (\alpha_k \rho_k \mathbf{v}_k \mathbf{v}_k) = -\alpha_k \nabla P + \nabla \cdot (\alpha_k \boldsymbol{\varepsilon}_k) + \Gamma_k \mathbf{v}_i + \mathbf{F}_k \quad (3)$$

where $\boldsymbol{\varepsilon}_k$ is the viscous stress. The balance of energy can be written as

$$\nabla \cdot [\alpha_k \rho_k H_{total,k} \mathbf{v}_k] = \nabla \cdot (\alpha_k \boldsymbol{\lambda} \nabla T_k) + \Gamma_k H_{total,i} + E_k \quad (4)$$

where $\alpha_k, \rho_k, \mathbf{v}_k, H_{total,k}, T_k$ are volume fraction, density, velocity vector, total enthalpy and temperature of the two phases. Γ_k, \mathbf{F}_k , and E_k are the interphase transfer of mass, momentum and energy, respectively. $\Gamma_k \mathbf{v}_i$ and $\Gamma_k H_{total,i}$ are the secondary momentum and energy sources (or sinks) related to mass transfer rate. \mathbf{v}_i and $H_{total,i}$ represent the quantities of the outgoing phase. For example, if vapor is generated, \mathbf{v}_i represents the velocity of liquid. Pressure jump at the interface is ignored.

The problem is set up and solved using CFX 18.2 by ANSYS. The working fluid is R134a. Liquid properties are assumed to be constant, which equals the inlet subcooled liquid properties. Redlich-Kwong real gas equation of state for R134a vapor has been used.

2.2 Nucleation Model

Because the degree of superheat in flashing cases is low, the contribution of homogeneous nucleation is ignored and the only contribution is assumed to be heterogeneous nucleation occurring on the walls.

Shin and Jones (1993) proposed an expression for departure radius of a bubble by balancing drag and surface tension forces:

$$R_d = 0.5787 K^{\frac{5}{7}} \left[\frac{\mu_l^{0.4}}{\tau_w^{0.7}} \sqrt{\frac{\sigma R_c}{\rho_l^{0.4}}} \right]^{5/7} \quad (5)$$

where K accounts for the fraction of the surface tension forces acting in opposition to the drag, μ_l is the liquid viscosity, τ_w is the wall shear stress, σ is the surface tension, R_c is the critical cavity radius, ρ_l is the liquid density. K was taken as unity in Shin and Jones (1993), which was also followed in the current study. Nucleation frequency was given as:

$$f = 10^4 [s^{-1} K^{-3}] (T_1 - T_{\text{sat}})^3 \quad (6)$$

where $T_1 - T_{\text{sat}}$ is the liquid superheat.

Riznic and Ishii (1989) proposed that the non-dimensional active nucleation site density which is defined as $N_{\text{ns}}^* = N_{\text{ns}} D_d^2$ can be correlated for flashing flow as:

$$N_{\text{ns}}^* = \left\{ \frac{2\sigma T_{\text{sat}}}{2(T_1 - T_{\text{sat}})\rho_v H_{\text{lv}}} \frac{D_d}{z} \right\}^{-4.4} f(\rho^*) \quad (7)$$

$$f(\rho^*) = C_{\text{surface}} \left(\frac{\Delta\rho}{\rho_v} \right)^{-3.12} \left(1 + 0.0049 \frac{\Delta\rho}{\rho_v} \right)^{4.13} \quad (8)$$

where $\Delta\rho = \rho_l - \rho_v$ and C_{surface} is a constant dependent on the surface nucleation property. Active nucleation site density increases as liquid superheat increases.

2.3 Interphase Transfer

It is assumed that phase change is induced only by interphase heat transfer due to thermal non-equilibrium between phases, which is called thermal phase change model in ANSYS CFX:

$$\Gamma_l = -\Gamma_v = \frac{\dot{Q}_l}{H_{\text{total},v} - H_{\text{total},l}} \quad (9)$$

The heat transfer rate is calculated using Newton's law of cooling

$$\dot{Q}_l = h_l (T_{\text{sat}} - T_1) A_{\text{int}} \quad (10)$$

where h_l is the overall heat transfer coefficient and A_{int} is the interfacial area density. In the current study, Hughmark's (1967) model is used for the estimation of interphase heat transfer coefficient. Vapor temperature is assumed to be equal to local saturation temperature. Therefore, there is no heat transfer between the vapor phase and the vapor-liquid interface. The interfacial area density is calculated by assuming that all the bubbles are spherical.

$$A_{\text{int}} = (6\alpha_v)^{\frac{2}{3}} (\pi N_b)^{\frac{1}{3}} \quad (11)$$

where N_b is the bubble number density. The mean bubble diameter can be calculated as:

$$D_m = \left(\frac{6\alpha_v}{\pi N_b} \right)^{\frac{1}{3}} \quad (12)$$

The local bubble number density equation can be expressed as:

$$\nabla(N_b v_b) = \phi_{\text{so}} - \phi_{\text{si}} \quad (13)$$

where ϕ_{so} , ϕ_{si} , and v_b are the bubble source term due to nucleation, the bubble sink term due to bubble collapse or coalescence and the local bubble velocity, respectively (Riznic and Ishii, 1989). In the current study, bubble nucleation is assumed to take place only at the nozzle wall. Bulk nucleation is neglected. Bubble collapse or coalescence are also neglected. The local bubble velocity is equal to the local vapor velocity. Interphase momentum transfer between the phases takes place due to the interfacial forces. In this study, drag, lift, and turbulent dispersion forces are considered. Schiller and Naumann's (1933) drag model, Saffman-Mei lift force model (1994), and Favre averaged drag model for turbulent dispersion (Burns *et al.*, 2004) have been used.

2.4 Turbulence Modeling

The RNG (Re-Normalisation Group) k- ϵ turbulence model with the standard wall-function has been used for liquid. The major differences between the standard k- ϵ turbulence model and the RNG model are the calculation of the turbulent viscosity in the case of the RNG model from the solution of an ordinary differential equation, which includes the effects of rotation and the presence of an additional term in the dissipation rate transport equation. Escue and Cui's (2010) work shows that RNG k- ϵ turbulence model gives good agreement with experimental results for swirling flow. Dispersed phase zero equation model is used for the estimation of the vapor eddy viscosity.

3. TEST CASES

The above model setup is tested with the conditions of experimental results published by Zhu and Elbel (2018a). The vortex nozzle tested by Zhu and Elbel (2018a) is composed of three components: a T-shaped part made of brass, a sleeve and a nozzle, both made of an optically clear resin and manufactured with a Stereo Lithography Apparatus (SLA), as shown in Figure 1. The tee-shaped part serves as the vortex generator. The tangential inlet on the tee allows flow to be injected tangentially and mix with the axial flow, thus creating a vortex. The tee and the nozzle are joined by a conical thread and sealed by epoxy adhesive. The geometric parameters of the vortex nozzle considered in the following simulation are presented in Table 1.

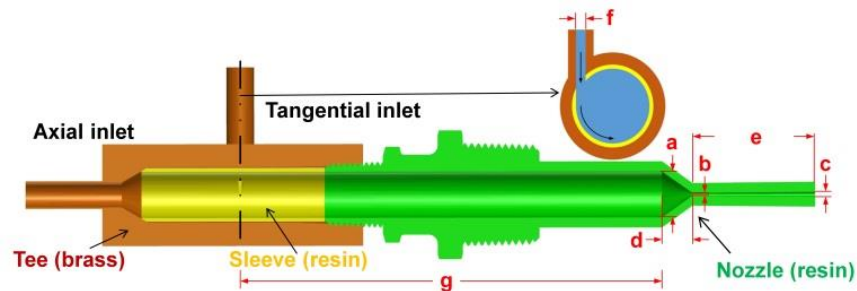


Figure 1: Vortex nozzle composed of tee, sleeve and convergent-divergent nozzle

Table 1: Vortex nozzle geometric parameters

(a) Nozzle inlet diameter (mm)	15.0
(b) Nozzle throat diameter (mm)	1.03
(c) Nozzle outlet diameter (mm)	1.07
(d) Nozzle convergent part length (mm)	9.9
(e) Nozzle divergent part length (mm)	2.1
(f) Tangential inlet inner diameter (mm)	2.0
(g) Vortex decay distance (mm)	168.0

The flow is steady state, compressible, and turbulent. The simulation is considered as converged when the maximal residual of all equations is below 10^{-5} and the maximum global imbalance is below 0.1%.

4. COMPUTATIONAL MESHES AND MESH STUDIES

In order to save computational costs, the fluid domain has been separated into two parts. The first part is mainly the vortex generator part. This part has two inlets, which are the axial and tangential inlets of the vortex nozzle, and one outlet, which is actually the inlet of the convergent-divergent nozzle. In this part the pressure is always above saturation pressure and therefore the fluid is single-phase liquid only.

The second part is the convergent-divergent nozzle part. The inlet and outlet of this part are basically the inlet and outlet of the nozzle. At the inlet, there is only single-phase liquid entering the domain. As the fluid goes through the nozzle, pressure drops below the saturation pressure and thus vapor is generated. This is where all the above-mentioned two-phase flow models have been applied. The outlet velocity profile of the vortex generator part for certain inlet mass flow rates combination is used as the inlet velocity profile of the nozzle part.

3D computational meshes are generated separately for the vortex generator part and the convergent-divergent nozzle part, as shown in Figure 2.

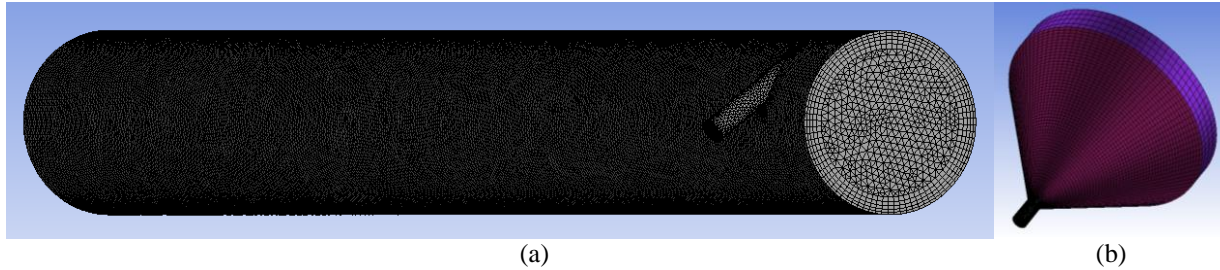


Figure 2: Mesh of (a) vortex generator part and (b) convergent-divergent nozzle part

In order to get mesh-independent results, mesh studies have been performed. For the vortex generator part, four meshes with different radial and axial resolution are investigated. The radial azimuthal velocity profiles at the vortex generator outlet for the four meshes with different numbers of nodes are presented in Figure 3. The tangential and axial inlet mass flow rates are 15.5 g/s and 0 g/s, respectively. The results achieved using the mesh with 362367 nodes can be considered as mesh-independent. In all the following simulations, this mesh is used for the vortex generator part. For the nozzle part, similarly four meshes with different radial and axial resolution have been generated and investigated. All the inlet conditions except for the inlet pressure as well as the outlet pressure are fixed. Table 2 shows the dependence of nozzle inlet pressure on the mesh resolution. Mesh 3 is considered as mesh-independent and is used for the nozzle part in the following simulation.

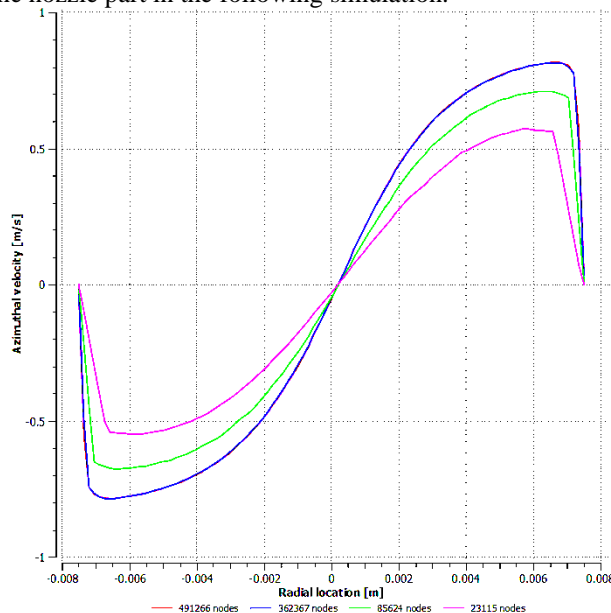


Figure 3: Radial azimuthal velocity profile at the vortex generator outlet for different numbers of nodes in the vortex generator part

Table 2: Results of mesh studies for the convergent-divergent nozzle part

Mesh no.	1	2	3	4
Total number of nodes	153367	242187	287413	491185
Nozzle inlet pressure (kPa)	962	909	897	896

5. PRELIMINARY SIMULATION RESULTS

Simulation has been run for the case with no inlet vortex and with maximum inlet vortex (all inlet mass flow going through the tangential inlet) under the conditions $P_{in}=920$ kPa, $T_{in}=36.0$ °C, as shown in Figure 4. No vapor is present at the nozzle inlet. $C_{surface}$ was set to $2.2E-5$ and turbulent dispersion coefficient of Favre averaged drag model for turbulent dispersion was set to 10 such that the mass flow rate errors between simulation and experimental results for the case with maximum inlet vortex are within 1.5% and that of the case with no inlet vortex are within

7%. According to the simulation, at the same nozzle inlet conditions and outlet pressure $P_{out} = 490$ kPa, the total mass flow rate through the nozzle has been reduced from 20.3 g/s with no inlet vortex to 17.5 g/s with maximum inlet vortex. This suggests that nozzle restrictiveness is increased after the application of inlet vortex, which shows good agreement with the experimental results.

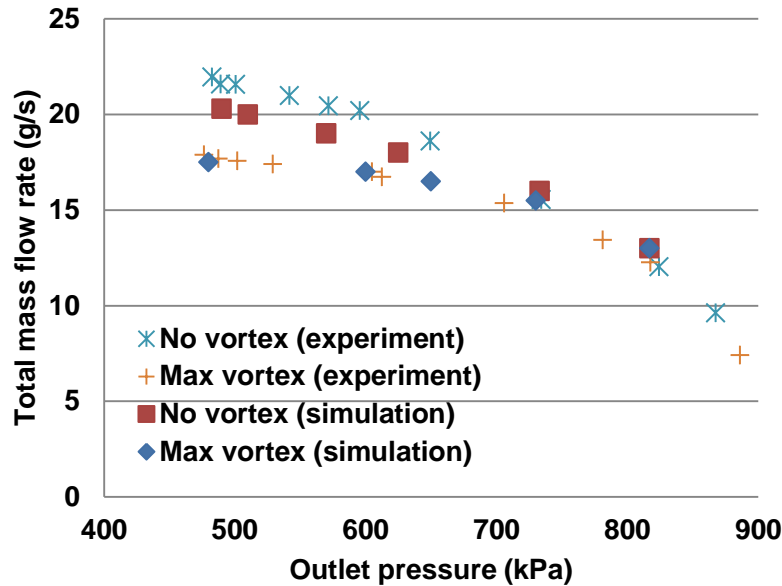


Figure 4: Comparison of experimental and simulation results without and with maximum inlet vortex at $P_{in} = 920$ kPa, $T_{in} = 36.0$ °C

Figure 5 shows the vapor volume fraction contour at the nozzle center plane generated by the simulation and the flow visualization by the experiment under similar conditions. In both cases, it can be observed that the flashing is started near the nozzle throat. The simulation result displays that there is negligible vapor content in the upstream of the throat even though the pressure is dropped below saturation pressure.

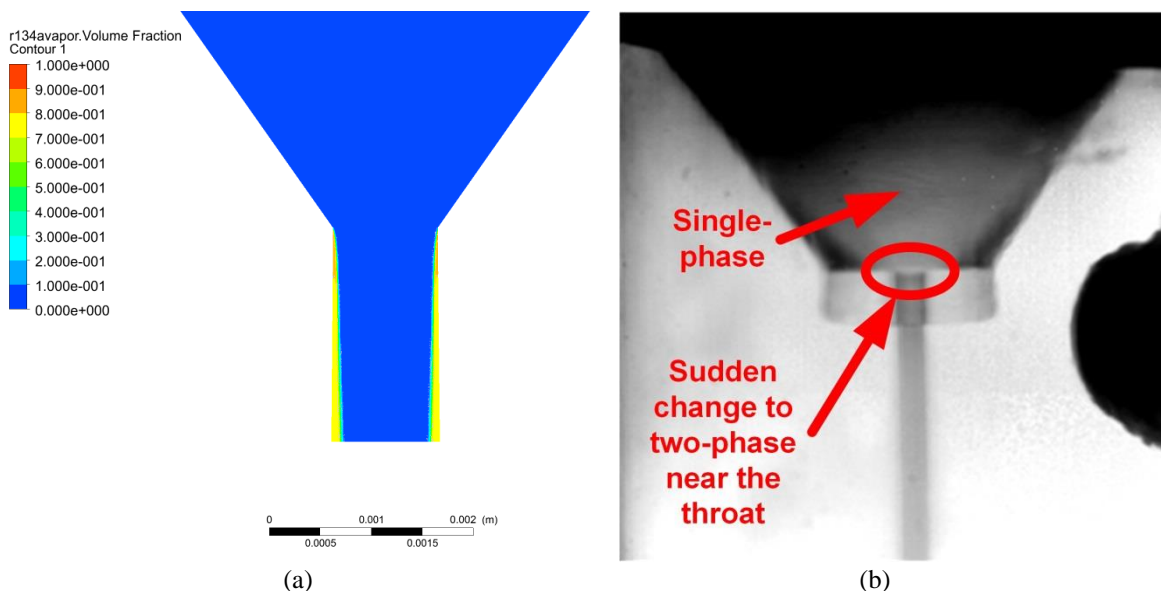


Figure 5: (a) Vapor volume fraction contour at the nozzle center plane by the simulation with $P_{in} = 920$ kPa, $T_{in} = 36.0$ °C, $P_{out} = 568$ kPa (b) flow visualization by experiment with $P_{in} = 915$ kPa, $T_{in} = 35.9$ °C, $P_{out} = 568$ kPa

Figure 6 compares the vapor volume fraction distribution at the nozzle outlet without and with maximum inlet vortex under similar conditions. It can be observed that vapor volume fraction is more concentrated near the wall when no vortex is applied. Due to the much lower density of vapor compared to the liquid, when vortex is applied vapor bubbles are driven towards the nozzle center. Therefore, after the application of inlet vortex, flow area at the nozzle outlet with vapor volume fraction larger than 0.1 is approximately two times that of the case without inlet vortex. The distribution of vapor volume fraction becomes less concentrated at the wall after the vortex is applied.

More vapor has been generated after the inlet vortex is applied. Vapor mass flow rate at the nozzle outlet has been increased from 0.19 g/s with no vortex to 0.34 g/s with maximum inlet vortex. The vapor quality at the outlet has been significantly increased from 0.9% to 1.9% after the application of inlet vortex. These results agree with the findings in Zhu and Elbel (2018b) that inlet vortex increases vapor generation in the divergent part of the nozzle.

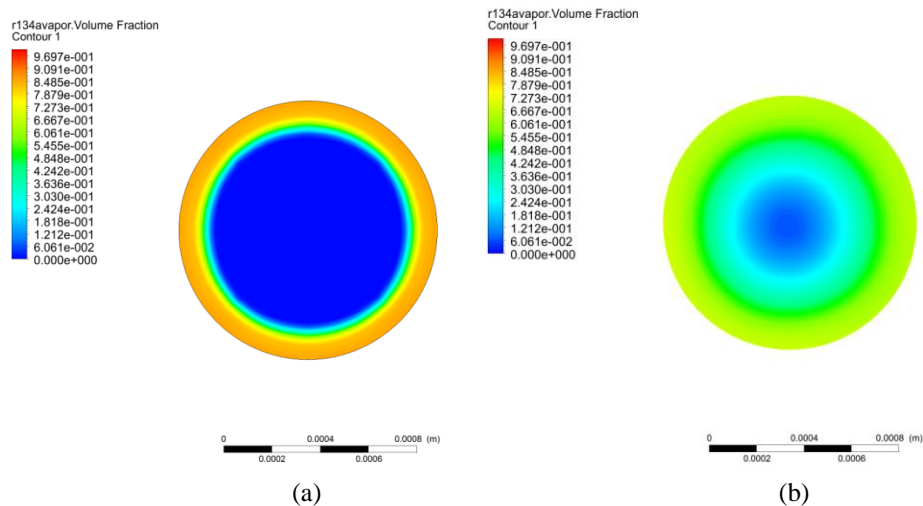


Figure 6: Vapor volume fraction at the nozzle outlet (a) with no inlet vortex at $P_{out} = 490$ kPa (b) with maximum inlet vortex at $P_{out} = 480$ kPa

Figure 7 displays the liquid temperature at different radial locations of the nozzle outlet without and with maximum inlet vortex. The region where noticeable decrease in liquid temperature can be observed (that is, liquid temperature is at least 0.1 K lower than the inlet liquid temperature 309.2 K (36.0 °C)) with maximum inlet vortex is much larger than that without inlet vortex. For the case with maximum inlet vortex, region with noticeable liquid temperature decrease at the nozzle outlet ranges from radial coordinate of 0.10 mm to the nozzle wall (radial coordinate of 0.54 mm), while that of the case with no vortex only ranges from radial coordinate of 0.40 mm to the nozzle wall. The decrease in liquid temperature represents the consumption of liquid sensible heat. The sensible heat of the liquid supplies the latent heat required by evaporator for bubble growth. Since the majority of the bubbles are near the wall when there is no vortex applied, the sensible heat of liquid near the wall is almost all depleted by the phase change. As vapor bubbles are driven towards the nozzle center due to the much lower density compared to liquid after the application of vortex, sensible heat of the liquid closer to the nozzle center can now be more utilized for bubble growth. Due to the more available liquid sensible heat, after the introduction of inlet vortex, vapor generation in the nozzle divergent part has thus been increased and flow control can be achieved.

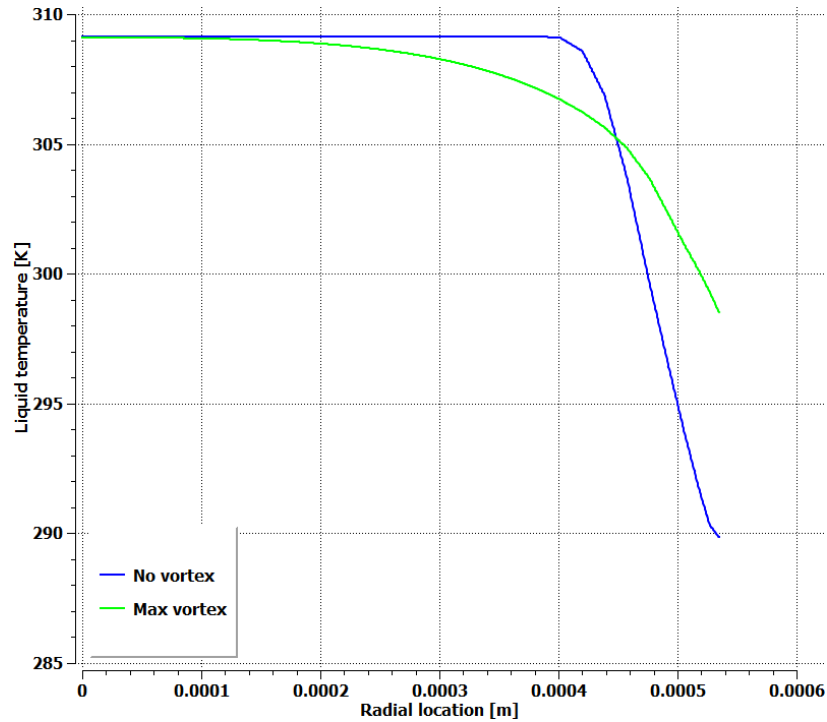


Figure 7: Nozzle outlet liquid temperature at different radial locations without and with maximum inlet vortex

6. CONCLUSIONS

In this paper, 3D CFD simulation of initially subcooled vortex flashing flows in convergent-divergent nozzles has been conducted. The simulation results show increase of nozzle restrictiveness after the application of inlet vortex, which agrees with the experimental results. The flashing is started near the nozzle throat. The simulation result displays that there is negligible vapor content in the upstream of the throat even though the pressure is dropped below saturation pressure. More vapor has been generated in the divergent part of the nozzle after the inlet vortex is applied. This is why the nozzle restrictiveness has been increased by the vortex. Due to the much lower density of vapor compared to the liquid, when vortex is applied vapor bubbles are driven towards the nozzle center. Sensible heat of the liquid closer to the nozzle center can now be more utilized for bubble growth. Due to the more available liquid sensible heat, after the introduction of inlet vortex, vapor generation in the nozzle divergent part has thus been increased and flow control can be achieved.

NOMENCLATURE

A	area density	(m ⁻¹)	ρ	density	(kg m ⁻³)
D	diameter	(m)	τ	shear stress	(Pa)
E	interphase energy transfer	(W m ⁻³)	σ	surface tension	(N m ⁻¹)
f	nucleation frequency	(Hz)			
F	interphase forces	(N m ⁻³)			
h	heat transfer coefficient	(W m ⁻² K ⁻¹)			
H	enthalpy	(J kg ⁻¹)			
P	pressure	(Pa)			
Q̇	heat transfer rate	(W m ⁻³)			
T	temperature	(°C)			
v	velocity	(m s ⁻¹)			
Greek Symbols			Subscript		
α	volume fraction	(-)	b	bubble	
Γ	mass transfer rate	(kg m ⁻³ s ⁻¹)	i	outgoing phase	
λ	thermal conductivity	(W m ⁻¹ K ⁻¹)	in	inlet	
μ	dynamic viscosity	(Pa s)	int	interfacial	
φ	source term	(m ⁻³ s ⁻¹)	l	liquid	
			m	mean	
			ns	nucleation site	
			out	outlet	
			sat	saturation	
			v	vapor	
			w	wall	

REFERENCES

- Burns, A. D., Frank, T., Hamill, I., and Shi, J. M., 2004, The Favre averaged drag model for turbulent dispersion in Eulerian multi-phase flows, *5th International Conference on Multiphase Flow*, vol. 4: p. 1-17.
- Escue, A., and Cui, J., 2010, Comparison of turbulence models in simulating swirling pipe flows, *Applied Mathematical Modelling*, vol. 34, no. 10: p. 2840-2849.
- Hughmark, G. A., 1967, Mass and heat transfer from rigid spheres, *AIChE Journal*, vol. 13, no. 6: p. 1219-1221.
- Mei, R., and Klausner, J. F., 1994, Shear lift force on spherical bubbles, *International Journal of Heat and Fluid Flow*, vol. 15, no. 1: p. 62-65.
- Riznic, J. R., and Ishii, M., 1989, Bubble number density and vapor generation in flashing flow, *International Journal of Heat and Mass Transfer*, vol. 32, no. 10: p. 1821-1833.
- Schiller, L. and Nauman, A., 1933, *V. D. I. Zeits*, vol. 77: p. 318.
- Shin, T. S. and Jones, O. C., 1993, Nucleation and flashing in nozzles-1. A distributed nucleation model, *International Journal of Multiphase Flow*, vol. 19, no. 6: p. 943-964.
- Zhu, J. and Elbel, S., 2016, A new control mechanism for two-phase ejector in vapor compression cycles for automotive applications using adjustable motive nozzle inlet swirl, *SAE Int. J. Passeng. Cars - Mech. Syst.*, vol. 9, no. 1: p. 44-51.
- Zhu, J. and Elbel, S., 2017, Influence of nozzle divergent part length and throat diameter on vortex control of initially subcooled flashing flow, *SAE Int. J. Passeng. Cars - Mech. Syst.*, vol. 10, no. 1: p. 121-127.
- Zhu, J. and Elbel, S., 2018, Experimental investigation of a novel expansion device control mechanism: Vortex control of initially subcooled flashing R134a flow expanded through convergent-divergent nozzles, *Int. J. Refrig.*, vol. 85: p. 167-183.
- Zhu, J. and Elbel, S., 2018, Measurement of pressure profile of vortex flashing flows in convergent-divergent nozzles, *17th International Refrigeration and Air Conditioning Conference at Purdue*, paper 2414.

ACKNOWLEDGEMENT

The authors would like to thank the member companies of the Air Conditioning and Refrigeration Center at the University of Illinois at Urbana-Champaign for their support.